EPJ Web of Conferences **182**, 02116 (2018) https://doi.org/10.1051/epjconf/201818202116
ICNFP 2017

Forward Physics at CMS

Sercan Sen[1,2,a,b]

[1] *Department of Physics Engineering, Hacettepe University, Ankara, Turkey*
[2] *The University of Iowa, Iowa City, USA*

Abstract. Recent forward physics measurements performed with the CMS detector at the LHC are reviewed. The measurements of the pseudorapidity dependence of the energy and transverse energy density, inclusive energy spectrum in the very forward direction, and the very forward inclusive jet cross sections are presented. The results are also compared to the predictions of various models used to describe high energy hadronic interactions.

1 Introduction

Measurements in the forward region are essential for a better understanding of the complete final states at the LHC [1]. In forward type of events, the particles are usually produced at small polar angles, θ, with respect to beam rapidity and the final states can contain large rapidity gaps devoid of hadronic activity. The CMS detector with its forward calorimeters as well as the beam line instruments allows to study a broad range of forward physics processes. The detailed description of the CMS detector can be found elsewhere [2]. The CMS Hadron Forward (HF) calorimeters are located on both sides of the interaction point and cover the pseudorapidity range $3.0 < |\eta| < 5.2$. The very forward calorimeter, CASTOR, is located only at one side of the CMS detector and covers the range $-6.6 < \eta < -5.2$ [3]. In the following, recent measurements performed with the HF and CASTOR calorimeters are presented.

2 Pseudorapidity dependence of the energy and transverse energy density

The energy flow in the forward pseudorapidities of the CMS detector, $3.15 < |\eta| < 6.6$, is measured in proton-proton (pp) collisions with a center-of-mass energy of $\sqrt{s} = 13$ TeV [4]. The low pile-up data were collected during a low luminosity running period at the very beginning of LHC Run 2 in 2015. The events were triggered with an unbiased trigger, based on the signals from BPTX detectors (The Beam Pickup Timing for the eXperiment), requiring only the presence of two colliding bunches at CMS. Two different strategies of event selection, single- and double-arm, are applied for the offline selection of events. The soft-inclusive inelastic events are selected by requiring a calorimeter tower above a threshold of 5 GeV in either side of HF (single-arm selection). The non-single diffractive

[a] e-mail: Sercan.Sen@cern.ch
[b] On behalf of the CMS Collaboration

enhanced events where the single-diffractive events are highly suppressed, are selected with a requirement of a calorimeter tower above a threshold of 4 GeV at both sides of HF (double-arm selection).

The forward energy flow is the sum of all energy deposits in the calorimeter towers above a noise threshold and is measured for two different event classes, soft-inclusive ineleastic and non-single diffractive enhanced events, using HF and CASTOR calorimeters. The measurement is corrected for all detector effects and the results are presented in the $3.15 < |\eta| < 6.6$ pseudorapidity range. The energy in the forward direction at stable-particle level is calculated by summing the energies of all particles, except muons and neutrinos, within the same pseudorapidity range of the measurement.

The energy flow as a function of η for soft-inclusive inelastic (left) and non-single diffractive enhanced (right) events are given with comparisons of the predictions of the models in Fig. 1. The gray band represents the total systematic uncertainty on the measurement, which is dominated by the uncertainty in the calorimeter energy scale of HF (10%) and CASTOR (15%). The energy flow in both soft-inclusive inelastic and non-single diffractive enhanced events increases with pseudorapidity and this feature is well described by all models.

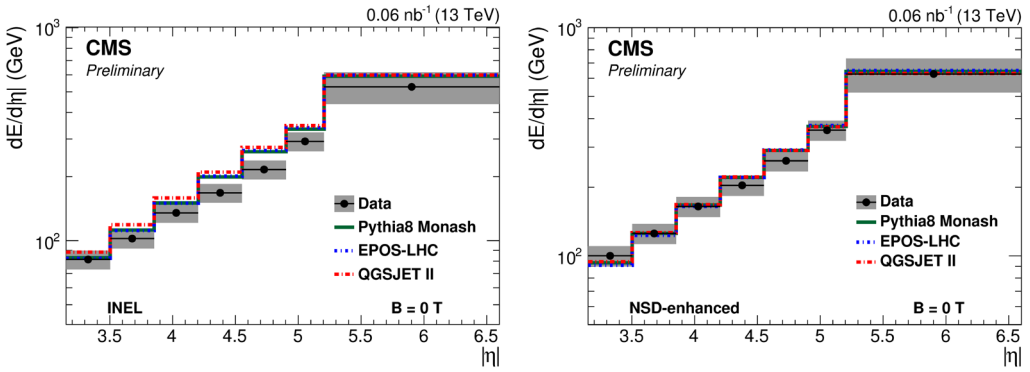

Figure 1. Energy flow as a function of η for soft-inclusive inelastic (left) and non-single diffractive enhanced (right) events at $\sqrt{s}$ = 13 TeV [4]. The gray band represents the total systematic uncertainty. The statistical uncertainties are negligible.

According to the hypothesis of limiting fragmentation in high energy hadron-hadron collisions, soft particle production is independent of center-of-mass energy in the beam fragmentation region, $\eta' \sim 0$ where $\eta' = \eta - y_{\text{beam}}$ ($y_{\text{beam}} = \ln(\sqrt{s}/m_p)$, the beam rapidity). To test this hypothesis, the transverse energy density ($dE_T/d\eta'$) as a function of $\eta - y_{\text{beam}}$ is shown in Fig. 2 together with the formerly published results at lower center-of-mass energies [5]. The results are also compared to the predictions of various models. The trends observed both in data and models favor the limiting fragmentation hypothesis.

3 Inclusive energy spectrum in the very forward direction

The differential cross section for inclusive particle production as a function of energy is measured in the CASTOR pseudorapidity acceptance, $-6.6 < \eta < -5.2$, in pp collisions at a center-of-mass energy of $\sqrt{s}$ = 13 TeV [6]. The analysis is based on the low pile-up data recorded at the beginning of LHC Run 2. An unbiased trigger, BPTX, is used to trigger the events. The events are further selected offline by requiring a calorimeter tower above a threshold of 5 GeV on either side of HF (single-arm event

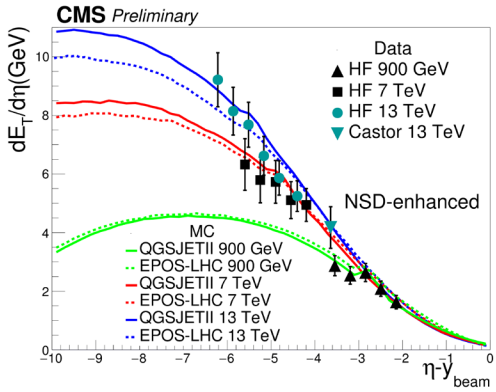

Figure 2. Transverse energy density ($dE_T/d\eta'$) as a function of $\eta - y_{\text{beam}}$ at different center-of-mass energies [4, 5]. Also shown as colored lines are the model predictions.

selection). The total energy in CASTOR is reconstructed by summing the energies of all calorimeter towers above the noise thresholds. The electromagnetic energy is reconstructed in the same way but only from the first two modules, and the hadronic energy is reconstructed from the last twelve modules. The measurements are corrected for all detector effects.

At stable particle level, the inclusive events are selected with a cut of $\xi > 10^{-6}$. The collection of stable final state particles (with $c\tau > 1$ cm) is divided into two systems, X and Y, based on the position of the largest rapidity gap in the event. The particles on the negative side of the gap are assigned to the system X. Similarly, the particles on the positive side of the gap are assigned to the system Y. The invariant masses, M_X and M_Y, of each system are calculated from the four-momenta of the particles in the X and Y systems, respectively. The $\xi_X = M_X^2/s$ and $\xi_Y = M_Y^2/s$, where s is the squared center-of-mass energy, are calculated. The variable ξ is defined as the maximum of ξ_X and ξ_Y.

For the total energy, all stable final state particles in $-6.6 < \eta < -5.2$, except muons and neutrinos, are taken into account. The electromagnetic energy is calculated from the energies of electrons and photons. Those particles are excluded when calculating the hadronic energy spectrum.

The fully corrected differential cross section as a function of total energy in CASTOR is given in Fig. 3 along with the comparisons of various Monte Carlo event generators commonly used in high energy cosmic ray physics (left panel) and those of different tunes of PYTHIA8 [7] (right panel). None of the models are able to describe the data over the whole range. The data is found to be very sensitive to the modeling of multiple parton interactions (MPI) and the prediction without MPI (red dashed-line on the right panel) is ruled out by the data.

The electromagnetic and hadronic energy spectra are given in Fig. 4 and Fig. 5 respectively.

4 Very forward inclusive jet cross section in pp collisions

The differential jet production cross section in the CASTOR pseudorapidity acceptance is measured in pp collisions with a center-of-mass energy of $\sqrt{s} = 13$ TeV [8]. The data were collected at the beginning of LHC Run 2 with an unbiased trigger requiring only the presence of two colliding bunches at CMS. The events are further selected offline only with a requirement of a jet reconstructed in CASTOR. As CASTOR has no resolution in η, all CASTOR calorimeter towers are assigned to a central

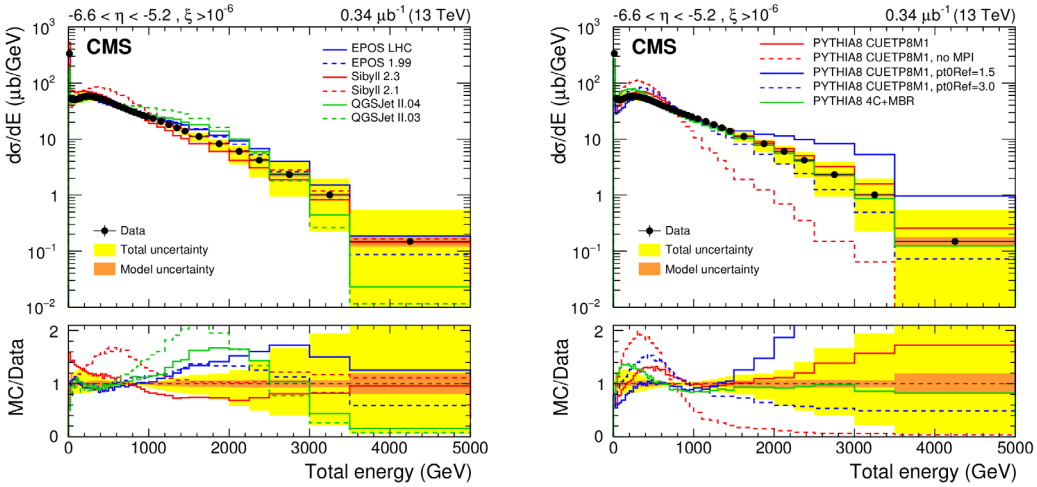

Figure 3. The differential cross section as a function of the total energy in CASTOR for events with $\xi > 10^{-6}$ [6]. On the left hand side, the spectrum is compared to the predictions of various Monte Carlo event generators commonly used in high energy cosmic ray physics, and on the right-hand side it is compared to those of different PYTHIA8 tunes.

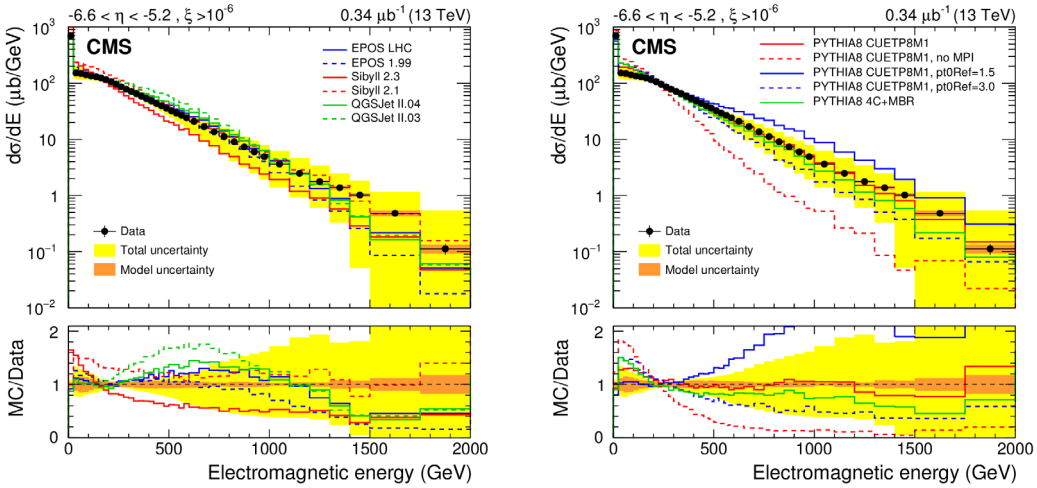

Figure 4. The differential cross section as a function of the electromagnetic energy in CASTOR for events with $\xi > 10^{-6}$ [6]. On the left hand side, the spectrum is compared to the predictions of various Monte Carlo event generators commonly used in high energy cosmic ray physics, and on the right-hand side it is compared to those of different PYTHIA8 tunes.

pseudorapidity value of the calorimeter which is $\eta = -5.9$. Jets are reconstructed from calorimeter towers using the anti-k_t clustering algorithm with a radius parameter of $R = \sqrt{\Delta\phi^2 + \Delta\eta^2} = 0.5$. The

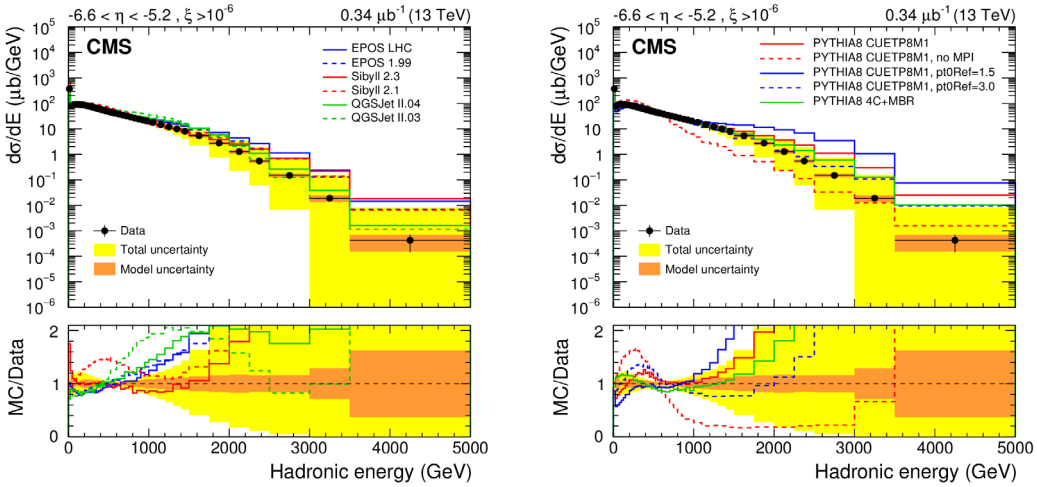

Figure 5. The differential cross section as a function of the hadronic energy in CASTOR for events with $\xi > 10^{-6}$ [6]. On the left hand side, the spectrum is compared to the predictions of various Monte Carlo event generators commonly used in high energy cosmic ray physics, and on the right-hand side it is compared to those of different PYTHIA8 tunes.

clustered jet energy, E_{jet}, is then converted to p_{T} of the jet with $p_{\text{T}} = E_{\text{jet}} / cosh(5.9)$. The measurement is corrected for all detector effects down to $p_{\text{T}} \approx 3$.

The differential jet production cross section and the jet yield in CASTOR (normalized by the number of visible jets in CASTOR) are given in Fig. 6. The energy scale uncertainty of CASTOR is the dominant uncertainty on the results, which is shown with yellow bands in the plots. The results are compared to the predictions of various models. All models agree with the data within the uncertainties. All PYTHIA flavors slightly overestimate the data, while EPOS-LHC [9, 10] and QGESJetII-04 [11, 12] tend to predict a softer spectrum with increasing p_{T}. It is also found that the results are very sensitive to the modeling of multiple parton interactions.

5 Very forward inclusive jet cross sections in p+Pb collisions

The differential jet energy cross section (as a function of jet energy) in the CASTOR pseudorapidity acceptance, is measured in p+Pb (proton towards CASTOR) and Pb+p (ion towards CASTOR) collisions with a center-of-mass energy of $\sqrt{s_{NN}} = 5.02$ TeV. In addition, the ratio of differential jet energy cross sections for p+Pb/Pb+p, which largely cancels out the systematic uncertainties in the measurement, is presented [13].

The data were collected in 2013 with a minimum bias trigger that required a track in central pseudorapidity ($|\eta| < 2.5$) with $p_{\text{T}} > 0.4$ GeV. To suppress the contribution from photon-induced and diffractive events, a further offline selection is performed by requiring an activity in HF above a 4 GeV threshold, on both sides (double-arm) with respect to the CMS interaction point. This non-diffractive type event selection is also adopted to stable-particle level by requiring a particle on both sides of the HF acceptance ($3 < |\eta| < 5$) with a minimal energy of 4 GeV, and a charged particle in the central acceptance with a $p_{\text{T}} > 0.4$ GeV. Jets in CASTOR are reconstructed with the anti-k_t jet clustering

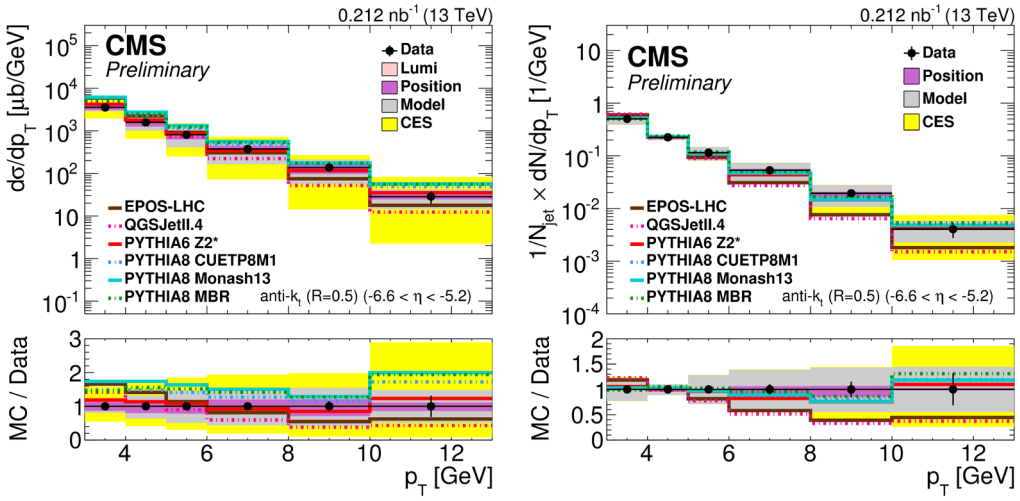

Figure 6. The differential jet production cross section in CASTOR (left) and the jet yield in CASTOR (right) [8].

algorithm with a radius parameter of $R = 0.5$. The measured jet energy is corrected for all detector effects.

The differential jet energy cross sections in CASTOR for p+Pb and Pb+p collisions are given in Fig. 7. The results are presented for energy ranges from 600 to 2500 (p+Pb) and to 4000 (Pb+p) GeV. The dominant source of the uncertainty on these results are the energy scale of CASTOR with 15%. The measured spectra are compared to the predictions of HIJING [14], EPOS-LHC, and QGSJETII-04. These generators do not include photon-induced processes, namely γp and $\gamma\gamma$, and HIJING does not include diffractive processes. The p+Pb data is well described by HIJING over the whole range, while EPOS and QGSJET progressively underestimate the data with increasing jet energies. The Pb+p data is underestimated by all models up to 1.2 TeV. The discrimination between data and models at higher jet energies of the Pb+p data is not perfect due to the large uncertainty on the energy scale of CASTOR. In the ratio of differential jet energy cross sections in CASTOR for p+Pb/Pb+p, the energy scale uncertainty largely cancels out and allows for a better discrimination between data and models. This is shown in Fig. 8. None of the models describe the full spectrum. HIJING describes the shape well but is not good in normalization. This finding clearly indicates that HIJING underestimates the high energy part in Pb+p data.

6 Summary

Recent measurements (mostly from Run 2) in the forward and very forward pseudorapidities of CMS are presented. Results are found to be sensitive to underlying event (UE) settings and provide valuable inputs for tuning of Monte Carlo event generators. Comparisons with earlier measurements can help to reveal the energy dependence of UE parameters. Jet reconstruction in CASTOR ($-6.6 < \eta < -5.2$) and measurements in both pp and pA collisions possess a unique sensitivity to nonlinear evolution effects.

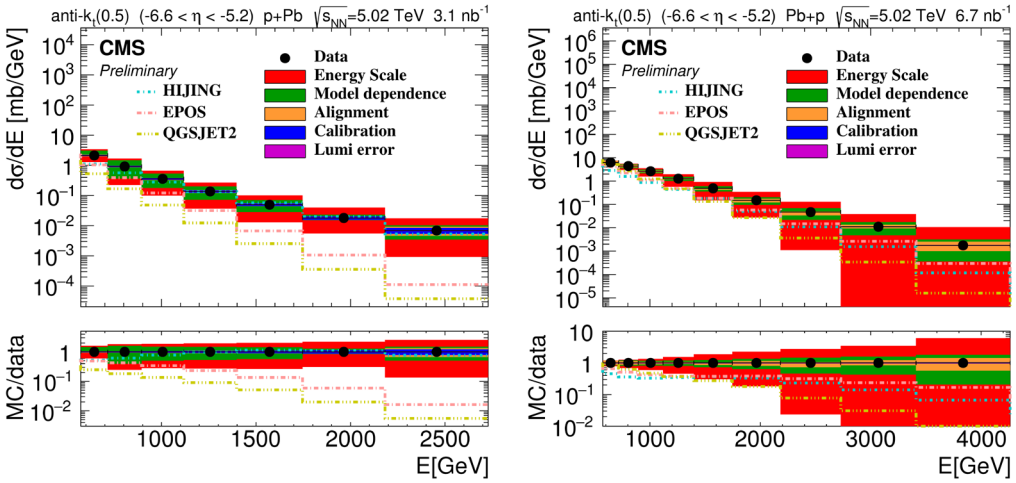

Figure 7. The differential jet energy cross section as a function of the jet energy in the region -6.6 < η < -5.2 for p+Pb collisions with the proton towards CASTOR (left) and for Pb+p collisions with the ion towards CASTOR (right) [13]. Note that the energy scale uncertainty is the dominant which is represented with the red band.

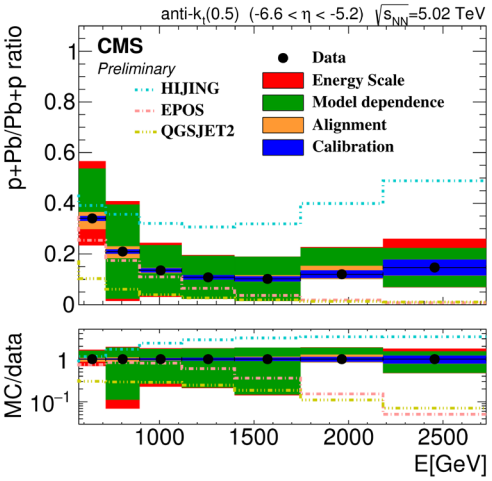

Figure 8. The ratio of differential jet energy cross sections as a function of the jet energy in the region -6.6 < η < -5.2 for p+Pb/Pb+p [13]. The model dependence uncertainty, represented with the green band, is the dominant.

7 Acknowledgments

This work was supported by Hacettepe University, Scientific Research Projects Program through the Project: FED-2017-14358.

References

[1] K. Akiba *et al.* [LHC Forward Physics Working Group], J. Phys. G **43**, 110201 (2016).
[2] CMS Collaboration, JINST **3**, S08004 (2008).
[3] V. Andreev *et al.*, Eur. Phys. J. C **67**, 601 (2010).
[4] CMS Collaboration, CMS-PAS-FSQ-15-006, https://cds.cern.ch/record/2146007 (2016).
[5] CMS Collaboration, JHEP **1111**, 148 (2011) Erratum: [JHEP **1202**, 055 (2012)].
[6] CMS Collaboration, JHEP **1708**, 046 (2017).
[7] T. Sjöstrand *et al.*, Comput. Phys. Commun. **191**, 159 (2015).
[8] CMS Collaboration, CMS-PAS-FSQ-16-003, https://cds.cern.ch/record/2146006 (2016).
[9] K. Werner, F. M. Liu and T. Pierog, Phys. Rev. C **74**, 044902 (2006).
[10] T. Pierog *et al.*, Phys. Rev. C **92**, no. 3, 034906 (2015).
[11] S. Ostapchenko, Phys. Rev. D **83**, 014018 (2011).
[12] S. Ostapchenko, Nucl. Phys. Proc. Suppl. **151**, 143 (2006).
[13] CMS Collaboration, CMS-PAS-FSQ-17-001, https://cds.cern.ch/record/2258273 (2017).
[14] X. N. Wang and M. Gyulassy, Phys. Rev. D **44**, 3501 (1991).